


Methodology for Controlling Unmanned Aerial Vehicle Landing on a Ground Wheeled Robot Tethered by Cable

Eduard Kuris^{1,*} , Konstantin Lelkov¹ , Timofey Khorev¹ 

¹.Moscow Aviation Institute  – Control Systems, Informatics and Electric Power Engineering – Flight-navigation and Information-Measuring Complexes – Moscow – Russian Federation.

*Correspondence author: eduardkuris@rambler.ru

ABSTRACT

For a robotic heterogeneous complex (RHC) consisting of a ground wheeled robot (GWR) and an unmanned aerial vehicle (UAV) connected by a tether mechanism (TM) and subject to steady wind acting on the UAV, a methodology for selecting control parameters for UAV landing on the GWR is considered. Landing is proposed along the straight line connecting the tether attachment point on the UAV with its base on the GWR. A synthesis of control for the TM and UAV engines was carried out to ensure landing within a predetermined time. A corresponding mathematical model of UAV and TM motion was derived. It is shown that the UAV's equilibrium positions along the line are stable, ensuring minimal engine energy consumption during landing. A synthesis of piecewise-linear damping coefficients in the control systems for the TM and UAV engines was performed by selecting moments of slope change based on synchronizing the instantaneous tether length and the distance from the UAV to the landing point. Simulation of the full equations of motion confirmed the feasibility of the proposed UAV landing methodology on the GWR and the validity of the assumptions made.

Keywords: Unmanned aerial vehicles (UAVs); Aerospace vehicle landing; Wind effects; Tether systems; Control systems.

INTRODUCTION

A heterogeneous system (RHS) consisting of a wheeled unmanned ground vehicle (UGV) and an unmanned aerial vehicle (UAV) connected by tether mechanism (TM) is undoubtedly an advanced development (Aleshin *et al.* 2020; Alonso Tabares and Mora-Camino 2017) for the purpose of monitoring the entire outer surface of an aircraft in its parking lot. With the help of such an RHS, monitoring is carried out simultaneously by cameras installed on both the UAV and the wheeled UGV (Cantelli *et al.* 2013; Kim *et al.* 2019; Wang L *et al.* 2020). When using such a wheeled UGV to inspect the aircraft surface, a critical factor is ensuring the operation of the TM, which guarantees the UAV collision avoidance with the aircraft under extreme wind impact conditions. In this case, both wind effects and TM forces act as external disturbances for the UAV, and its onboard control system must compensate them to a significant extent to ensure stable flight. The issue of compensation for external disturbances of UAV are widely covered in various studies (Liu *et al.* 2024; Uzun and Oktay 2023). There are differential methods of wind impacts in the UAV control system. However, these methods have natural constraints associated with limiting the maximum propellers' thrust of UAV (Chodnicki *et al.* 2022; Krishnakumar *et al.* 2015; Wang B *et al.* 2020). Generally, the UAV and the aircraft collision avoidance can be ensured if the aerodynamic force from the wind impact on the UAV is counteracted not only by the UAV propellers' forces, but

Received: Oct. 02, 2024 | **Accepted:** Jan. 27, 2025

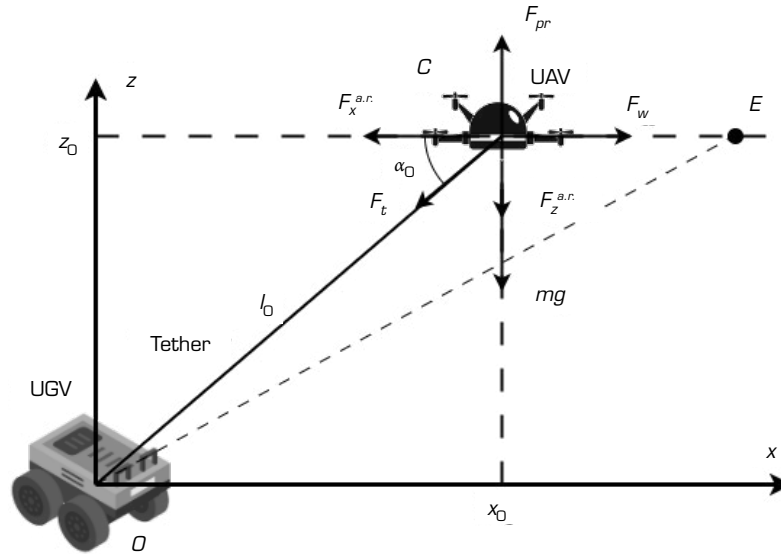
Peer Review History: Single Blind Peer Review.

Section editor: Paulo Renato Silva 



also by the forces generated by the power-guided TM engine to a considerable degree. Moreover, it is assumed that the design of the TM is chosen so that the maximum force exerted by it is greater than the maximum force from the possible wind impact on the UAV.

A diagram illustrating the force distribution applied to a multi-rotor UAV when held by TM is shown in the Fig. 1 (Aleshin *et al.* 2020).



Source: Adapted from Aleshin *et al.* (2020).

Figure 1. Scheme of forces distribution applied to the UAV in the process of counteracting extreme wind impact. $O_a x_a z_a$ is a coordinate system (CS), rigidly connected with UAV (O_a is UAV's center of mass, axis $O_a x_a$ is horizontal and applied normal to the UAV trajectory towards the outer surface of the aircraft, axis $O_a z_a$ is applied to the position vertical); Oxz is CS centered at O in the wheeled UGV's center of mass (its axes are parallel to the corresponding CS axes $O_a x_a z_a$), O also coincides with the place of tether attachment in the TM; C is the starting point at which the UAV is located before a gust of wind and where it returns before landing, (its coordinates x_0, z_0); l_0 is the tether segment length from the wheeled UGV to the UAV when it is located at the point C; F_w is the aerodynamic force created by the wind load on the UAV; F_t is the force acting on UAV from the tether side; F_{pr} is the thrust created by the rotors (Aleshin *et al.* 2020); mg is the UAV gravity (m is the UAV mass, g is the gravity acceleration); F_x, F_z is the drag force acting on the UAV, respectively, along the axes X_a, Z_a ; α_0 is the tether tilt angle with the respect to the horizon plane when the UAV is located at the point C.

In Fig. 1, the motion from the point C (after the beginning of the wind load action) to the point E and inversely occurs according to a certain algorithm given in Aleshin *et al.* (2020) and including mainly the operation of the TM engine with the withdrawing the tether to its maximum value at point E (located directly next to the surface of the aircraft) and the subsequent UAV return to the point C where it is in an equilibrium position.

The objective of this study is to analyze the possibility and synthesis of TM and UAV control systems under conditions of the unchanged direction of the wind impact, in which the UAV is pulled up to the landing place on the wheeled UGV along the line connecting the point C of the UAV's initial location and the tether's attachment place O. This is done by organizing its motion along a straight line OC to such a height in the vicinity of the point O from which the landing can be carried out without the participation of TM in accordance with the landing algorithm of the control system of the UAV itself.

Theoretical basis

The mathematical model of the RHS under the specified motion conditions can be considered as a combination of the motion model of the UAV's center of mass and the TM's mathematical model with a DC motor (Aleshin *et al.* 2020):

$$\begin{aligned}
m\ddot{x} &= F_w - F_t \cos \alpha - F_x^{a.r.}; \\
m\ddot{z} &= F_{pr} - F_t \sin \alpha - F_z^{a.r.} - mg; \\
\alpha &= \arccos \frac{x}{\sqrt{x^2 - z^2}}; \\
L_c \dot{I} + R_c I &= U - c_{cef} \omega_c; \\
(J + mr_c^2) \dot{\omega}_c + \varepsilon \omega_c &= M_{met} - \left((F_w \cos \alpha - F_x^{a.r.}) + (F_{pr} - mg) \sin \alpha \right) r_c; \\
M_{met} &= nI; \\
F_t &= \frac{M_{met}}{r_c},
\end{aligned} \tag{1}$$

where x, z are the coordinates of the UAV center of mass in the CS Oxz , α is the tether tilt angle with the respect to the horizon plane, U is the control voltage on the motor, I is the current in the motor drive winding, ω_c is the angle rate of the shaft rotation of the motor with the coil ($\omega_c > 0$ when winding the tether on the coil), M_{met} is the electromagnetic torque on the motor shaft, J is the moment of inertia of the motor shaft with the coil, ε is the torque coefficient of the viscous friction around the axis of the motor shaft's rotation, L_c, R_c are the inductive property and resistance of the motor control winding, respectively, C_{cef} is coefficient of counter-electromotive force, n is the torque constant of the motor, and r_c is the average radius of the coil with the tether.

The forces of aerodynamic air resistance $F_x^{a.r.}, F_z^{a.r.}$ directed by true airspeed are determined by the ratios:

$$F_i^{a.r.} = c_{di} \frac{\rho v_i^2}{2} S_i, i = x, z, \tag{2}$$

where c_{di}, v_i are the non-dimensional aerodynamic coefficients and true airspeed in the corresponding axes' direction, S_i are the UAV's effective surface areas normal to the corresponding axes, and ρ is the air density.

In the current study, the aerodynamic characteristics of the UAV were determined experimentally, but in general, this can also be done based on modeling (Xie *et al.* 2022).

METHODOLOGY

Determining the stable position line of the UAV during landing

As mentioned above, upon condition $\alpha = \alpha_0$, the UAV is located at point C in the equilibrium position, while the required tether tension F_t and lift F_{pr} can be expressed in terms of a known wind force's constant F_w as follows:

$$\begin{aligned}
F_t &= F_w / \cos \alpha; \\
F_{pru} &= F_w \tan \alpha_0 = F_{pr} - mg.
\end{aligned} \tag{3}$$

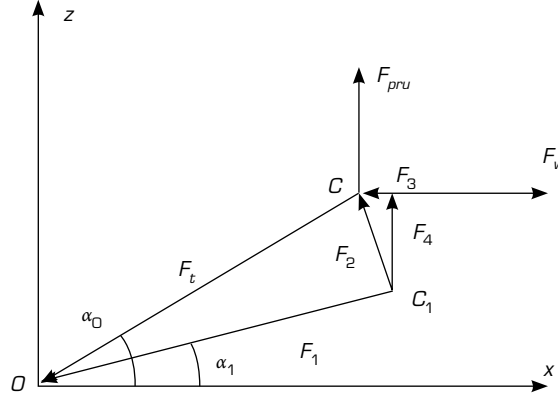
It follows from Eq. 1 that the force F_t corresponds to a motor's constant control voltage U_0 equal to:

$$U_0 = F_t R_c \frac{r_c}{n}. \tag{4}$$

From Eqs. 1 and 3, it is seen that when the UAV is located on a straight axis OC, the ratio is fulfilled for each of its points (x, z):

$$\frac{x}{\sqrt{x^2 + z^2}} = \frac{x_0}{\sqrt{x_0^2 + z_0^2}} \quad (5)$$

At the same time, the values of the forces F_t and F_{pru} will not change. Thus, at each point of the OC line, when performing Eqs. 3 and 5, the UAV will be in the equilibrium position. It must be shown that this position is stable. Figure 2 shows the forces acting on the UAV at the starting point C (F_t) and at its random displacement to the point C_1 (F_w).



Source: Elaborated by the authors.

Figure 2. Forces' distribution when the UAV is displaced from C to C_1 .

Note that the absolute value of F_1 is equal to the absolute value of F_t . In this case, a force F_2 arises such that:

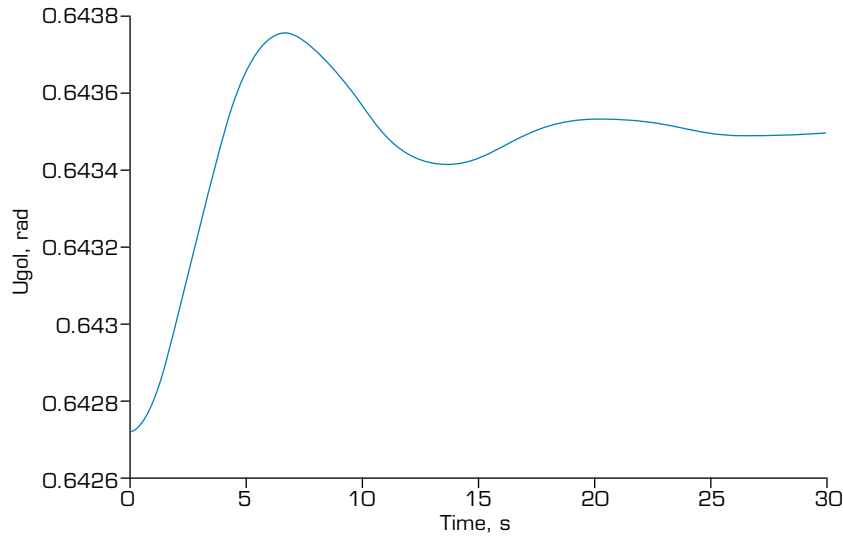
$$\mathbf{F}_t = \mathbf{F}_1 + \mathbf{F}_2. \quad (6)$$

In its turn, F_2 is decomposed into components – vertical F_3 and horizontal F_4 , the impact of which returns the UAV to a straight line $\alpha = \alpha_0$. Under the effect of these forces, oscillations occur simultaneously along the horizontal and vertical axes. With damping, the UAV will return to the equilibrium position at the angle $\alpha = \alpha_0$, although the UAV's coordinates may change both vertically and horizontally. This equilibrium position satisfies the Lyapunov stability criterion (Pukdeboon 2011). The system's simulation of the first three equations in Eq. 1 was carried out when performing Eq. 3 to validate the stability of the UAV's straight-line $\alpha = \alpha_0$ equilibrium positions, considering the introduction of damping terms.

$$\begin{aligned} m\ddot{x} &= F_w - F_t \cos \alpha - F_x^{a.r.} - k\dot{x}; \\ m\ddot{z} &= F_{pru} - F_t \sin \alpha - F_z^{a.r.} - k\dot{z}; \\ \alpha &= \arccos \frac{x}{\sqrt{x^2 + z^2}}, \end{aligned} \quad (7)$$

where $k\dot{x}, k\dot{z}$ are the damping forces formed in the UAV engine control system when it is displaced along the corresponding coordinate axes. It is worth noting that to determine the tether tilt angle α in Eq. 7, it is necessary to ensure the determination of high-precision navigation parameters of the UAV and the wheeled UGV. In particular, robust inertial guidance algorithms can be used regarding to the use of the wheeled UGV and UAV near the aircraft's surface, where there are significant distortions of satellite navigation signals (Antonov *et al.* 2017; Veremeenko *et al.* 2020; 2021; Zharkov *et al.* 2022).

The simulation result for $m = 6$ kg, $F = 30$ N, $c_d = 0,15$, $c_{dx} = 0,12$, $S_x = 0,04$ m², $S_t = 0,03$ m², $k = 2$ N·s, $x_0 = 20$ m, $z_0 = 15$ m, $\alpha_0 = 0,6435$ rad and initial conditions $x = 21$ m, $z = 15,5$ m is shown in Fig. 3 (the quantities' steady-state values are $\alpha = \alpha_0$, $x = 20,38$ m, $z = 15,29$ m).



Source: Elaborated by the authors.

Figure 3. Angle change α in case of accidental UAV's deviation from the line $\alpha = \alpha_0$.

Synthesis of TM control

Define the required additional control voltage $k_u \cdot U_0$ on the TM engine in Eq. 2 corresponding to the desired UAV's landing time t_b on the wheeled UGV. Introduce the notations:

$$\begin{aligned} U &= U_0 + k_u U_0; \\ I &= I_0 + k_i I_0; \\ F_t &= F_0 + k_f F_0, \end{aligned} \quad (8)$$

where U_0 and I_0 are the steady-state values of voltage and current in the TM motor corresponding to the tether's tension force in the equilibrium position at the angle I_0 and k_u, k_p, k_f are coefficients setting the corresponding control points. For clarity of further compilations, Eq. 1 is transformed by introducing the following terms: $F_0 \cos \alpha_0 - F_0 \cos \alpha$ in the Eq. 1 and $F_0 \sin \alpha_0 - F_0 \sin \alpha$ in the second one. Replacing now $F_w = F_0 \cos \alpha_0$, $F_{pru} = F_0 \sin \alpha_0$ and neglecting the aerodynamic forces' influence, the following is obtained with regard to Eq. 8:

$$\begin{aligned} m\ddot{x} &= F_0 (\cos \alpha_0 - \cos \alpha) - k_f F_0 \cos \alpha; \\ m\ddot{z} &= F_0 (\sin \alpha_0 - \sin \alpha) - k_f F_0 \sin \alpha; \\ \alpha &= \arccos \frac{x}{\sqrt{x^2 + z^2}}; \\ L_c \dot{I} + R_c k_i I &= k_u U_0 - c_{cef} \omega_c; \\ (J + m r_c^2) \dot{\omega}_c + \varepsilon \omega_c &= n k_i I + F_0 (1 - \cos(\alpha_0 - \alpha)) r_c; \\ k_f F_0 &= k_i I \cdot n / r_c. \end{aligned} \quad (9)$$

For the landing time t_b analytical determination, it is assumed that $L_c \dot{I} = 0$ and neglect (based on preliminary numerical estimates) the last term in the fourth equation. Then, the third and fourth equations in Eq. 9 can be considered separately from the first three. Adding to them the obvious ratio connecting t_b with ω_c and the tether's length l_0 , get:

$$\begin{aligned}
R_c k_i I_0 &= k_u U_0 - c_{cef} \omega_c; \\
(J + m r_c^2) \dot{\omega}_c + \varepsilon \omega_c &= n k_i I_0; \\
l_0 &= r_c \int_0^{t_b} \omega_c dt; \\
l_0 &= \sqrt{x_0^2 + z_0^2}.
\end{aligned} \tag{10}$$

Finding from the first equation in Eq. 10 and inserting it into the second gives:

$$(J + m r_c^2) \dot{\omega}_c + (\varepsilon + n c_{cef} / R_c) \omega_c = n k_u \frac{U_0}{R_c}. \tag{11}$$

The solution of the linear differential Eq. 11 with $\omega_c(0) = 0$ is written as (Massera and Schäffer 1958):

$$\omega_c = a(1 - e^{-a_1 t}), \tag{12}$$

where $a = n k_u \frac{U_0}{(\varepsilon + n c_{cef} / R_c) \cdot R_c}$; $a_1 = \frac{\varepsilon + n c_{cef} / R_c}{J + m r_c^2}$.

Inserting Eq. 12 into the last equation in Eq. 10 and integrating, obtain the desired dependence between the landing time and the voltage control coefficient from Eq. 8:

$$l_0 = a r_c \left(t_b + (e^{-a_1 t_b} - 1) / a_1 \right) \tag{13}$$

or

$$k_u = (\varepsilon + n c_{cef} / R_c) R_c \frac{\frac{l_0}{r_c \left(t_b + \frac{e^{-a_1 t_b} - 1}{a_1} \right)}}{n} / U_0 \tag{14}$$

Estimate the formal time of the UAV's motion to the landing point in accordance with the first two equations in Eq. 9, assuming that the motion occurs along the line $\alpha = \alpha_0$. Then, taking into account Eq. 4, it will be as follows:

$$\begin{aligned}
m \ddot{x} &= -k_u U_0 \frac{n}{R_c} / r_c \cdot \cos \alpha_0; \\
m \ddot{z} &= -k_u U_0 \frac{n}{R_c} / r_c \cdot \sin \alpha_0.
\end{aligned} \tag{15}$$

Since each of these equations is a projection of the UAV's motion along the tether tension line on the corresponding axis, for the desired time t_d have the ratio:

$$t_d = \sqrt{\frac{2 x_0 m}{k_u U_0 \frac{n r_c}{R_c} \cos \alpha_0}}. \tag{16}$$

Calculations have shown that with the same UAV and TM parameters, the time of the UAV's motion to the landing point in accordance with Eq. 15 is significantly less than the time t_b of the tether's winding off by the TM engine in accordance with Eq. 10. This will lead to the tether's sagging, subsequent oscillations of the UAV and a complete disturbance of the landing mode in question. To maintain the proposed landing mode, the value and direction of the UAV engines' thrust were changed so that the times t_d and t_b coincided. Studies have shown that it is advisable to form these additional forces as damping ones – as a function of the UAV velocities according to the corresponding coordinates. Then, Eq. 15 will be as follows:

$$\begin{aligned} m\ddot{x} &= -f_{xd}\dot{x} - k_u U_0 \frac{nr_c}{R_c} \cos \alpha_0; \\ m\ddot{z} &= -f_{zd}\dot{z} - k_u U_0 \frac{nr_c}{R_c} \sin \alpha_0, \end{aligned} \quad (17)$$

where f_{xd}, f_{zd} are the corresponding functions at which the synchronization of the current tether length obtained by solving Eq. 10 and the current position of the UAV is carried out – the values of $L = \sqrt{x^2 + z^2}$ (the current distance from the position of the UAV to the point of intended landing) obtained by solving Eq. 17. The formation of forces $f_{xd}X$ and $f_{zd}Z$, for example, for a six-rotor UAV occurs due to the total thrust vectoring (Arellano-Muro *et al.* 2013). For an anticipatory appraisal of the motion's time of the UAV to the landing point, we will consider f_{xd} as a constant value. In this case, the equations' form of Eq. 17 coincides with Eq. 11, and the solution, for example, of the first equation in Eq. 17 at the initial value will be written as:

$$\dot{x} = c \left(t_d \frac{e^{-c_1 t_d} - 1}{c_1} \right), \quad (18)$$

where $c = -k_u U_0 \frac{nr_c}{R_c} \cdot \frac{\cos \alpha_0}{f_{xd}}$; $c_1 = \frac{f_{xd}}{m}$.

Then for the coordinate $x(t)$ at $x(0) = 0$ and $t = t_d$ get:

$$x(t_d) = ct_d + c \frac{e^{-c_1 t_d}}{c_1} + x_0 - \frac{c}{c_1}. \quad (19)$$

To simulate the landing process, it is necessary to set the time $t_b = t_d$. When choosing it, the following factors should be taken into account. It should be more than the time constant a_i in Eq. 11 and c_i in Eq. 18, which will make it possible to consider the tether's and the UAV's motion in the landing process as quasi-stationary, acceptable for practical implementation. At the same time, the least (minimum) energy should be spent when generating voltage on the TM engine and in engines that create thrust. A detailed study of this issue is beyond the scope of the article.

RESULTS

To evaluate the effectiveness of the proposed UAV landing control system, simulation was carried out. The obtained data illustrate the necessary degree of synchronization between the UAV's movement and the operation of the tether mechanism, which in turn ensures the appropriate quality of the landing process.

Set:

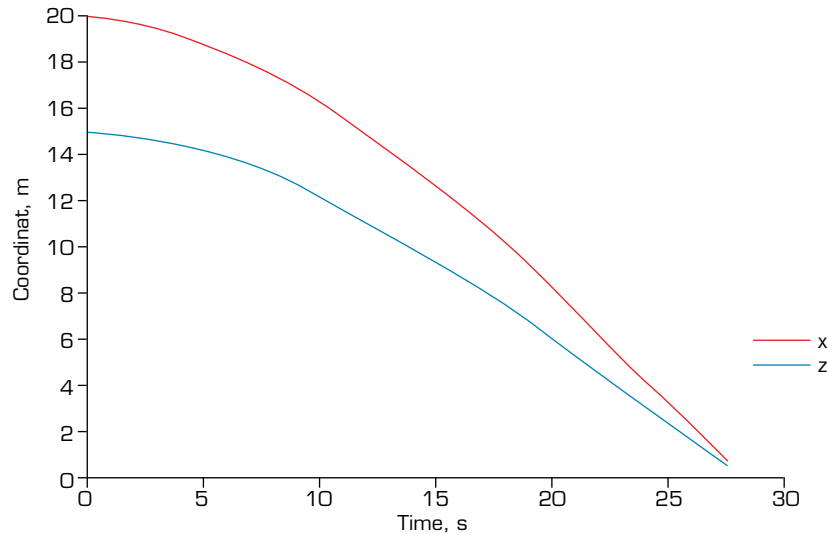
$$t_b = t_d = 60c. \quad (20)$$

For further calculations, the initial values of the UAV and TM parameters were assumed to be the same as in Aleshin *et al.* (2020): $\cos \alpha_0 = 0.8$; $J = 0.7 \text{ kgm}^2$; $m = 6 \text{ kg}$; $c_{dz} = 0.15$; $c_{dx} = 0.12$; $c_{cef} = 0.016 \text{ Vs/rad}$; $F_w = 30 \text{ N}$; $\varepsilon = 3 \cdot 10^{-3} \text{ Nm/rad}$; $n = 0.5 \text{ Nm/A}$; $I_0 = 25 \text{ m}$. When using the ratios Eq. 14 and Eq. 16 to achieve the minimum difference between t_d and t_b , the following results were obtained for the conditions: $R_c = 0.2 \text{ Ohms}$; $R_c = 0.3 \text{ m}$, while t_d increased from 10 s to 28 s. For $t_d = 60 \text{ s}$ from Eq. 19, the value was determined numerically, based on the division method of the segment in half (Tikhonov *et al.* 1995), obtained $f_{xd} = 0.916$ value and the following values in Eq. 8:



$$U_0 = 4.5 \text{ V}; I_0 = 22.5 \text{ A}; F_0 = 37.5 \text{ N}; k_u = 0.0102; k_j = 0.0102 \quad (21)$$

The graph of the UAV coordinate change obtained by solving Eq. 1 for the above parameters and values from Eq. 21 is shown in Fig. 4.



Source: Elaborated by the authors.

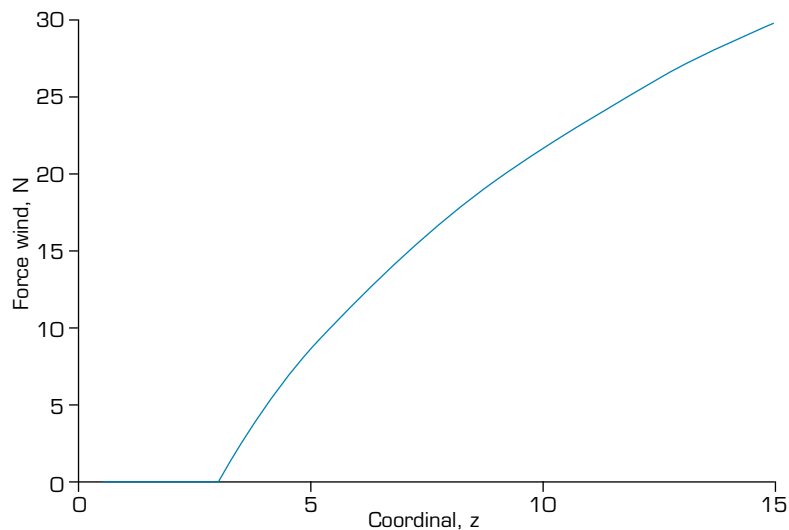
Figure 4. Changing the coordinates of the UAV in the motion process to the landing point.

Note that the motion time is close to the one set in Eq. 20. Simultaneously, near the landing point, the UAV's speed is unacceptably high.

Now, consider a situation where the wind force remains constant but its magnitude depends on the height above the Earth's surface (absolute altitude). Obviously, in the vicinity of the landing point, the wind force will decrease so much as that only the regular UAV control system will be sufficient for further landing. Let, for example, the dependence of wind strength on height be given by the function (Turgut and Usanmaz 2016):

$$F_w(z) = F_{w0} \left(\frac{z^{n/(2-n)} - z_2^{n/(2-n)}}{z_1^{n/(2-n)} - z_2^{n/(2-n)}} \right), \quad (22)$$

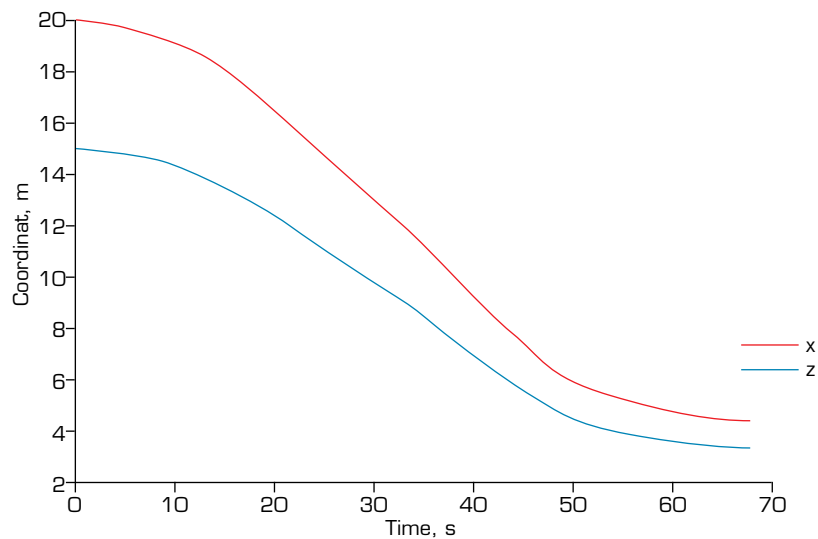
where F_w , F_{w0} are, respectively, the wind strength at the current height Z and the initial one Z_1 , Z_2 is the height at which $F_w = 0$, and n is a coefficient that takes into account the temperature gradient in height. The dependence graph Eq. 22 is shown in Fig. 5.



Source: Elaborated by the authors.

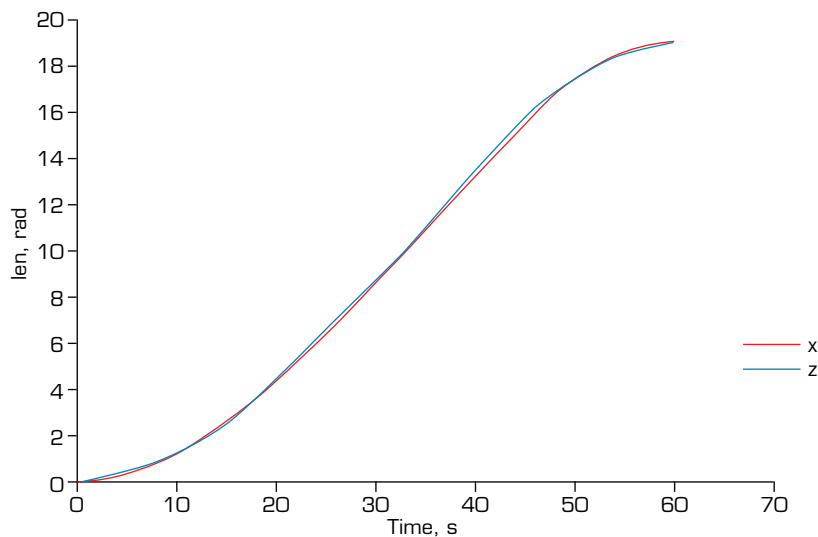
Figure 5. Wind strength dependence of an altitude ($z_1 = 3$).

Modeling of the landing process will be carried out according to the following algorithm. From height $z = z_1$ to $z = z_3$ ($z_3 > z_1$), landing occurs due to the attraction of the UAV along a line close to $\alpha = \alpha_0$, while the formation of the value of the control voltage $U = K_u U_0(Z)$ in Eq. 2 is carried out in accordance with the ratio (Eq. 4) (for $U_0(Z(t))$) and the coefficient k_u is determined from Eq. 14 and is constant throughout the entire motion from $z = z_1$ to $z = z_2$. The formation of coefficients f_{xd} and f_{zd} , as before, is made from the condition of ensuring synchronization of the current tether length and the UAV's position. At altitude $z = z_3$ only the voltage $U = U_0(z)$, corresponding to the wind force at altitude $z = z_3$ is applied to the TM engine, while damping forces $f_{zd}z$ and $f_{xd}x$ continue to form in the UAV engines. In this case, the UAV's speed gradually decreases and UAV's position becomes stable due to the UAV's stable position relative to the line $\alpha = \alpha_0$. However, under the action of inertia, the tether continues to wind off. To synchronize the tether's length with the UAV's coordinates, an appropriate compensating voltage is formed on the TM engine. The UAV hovers, then further landing is carried out with the TM engine turned off only due to the operation of the standard UAV control system. Figures 6–9 represent the results of modeling. Figures obtained on the basis of integration (Eq. 1) with the corresponding forming of functions f_{xd} and f_{zd} in Eq. 17 for $z_3 = 5$ m and the UAV and TM parameter values mentioned above.



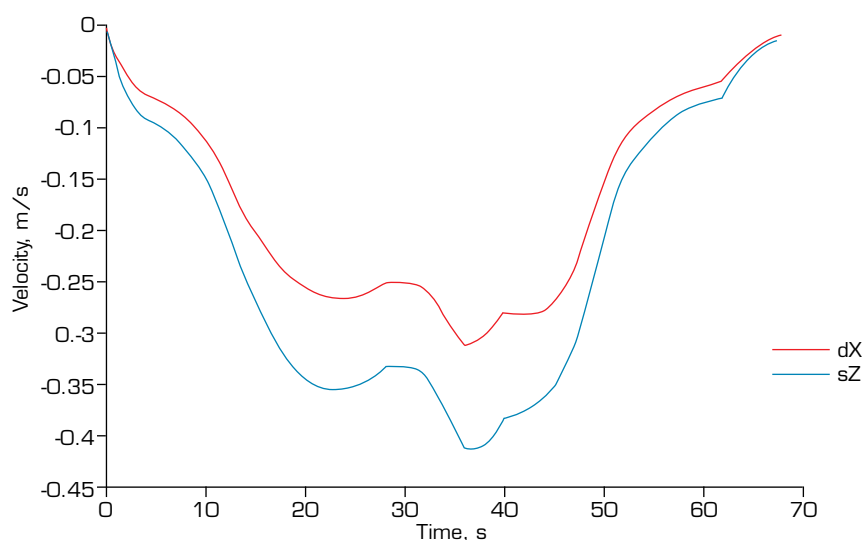
Source: Elaborated by the authors.

Figure 6. UAV coordinates.



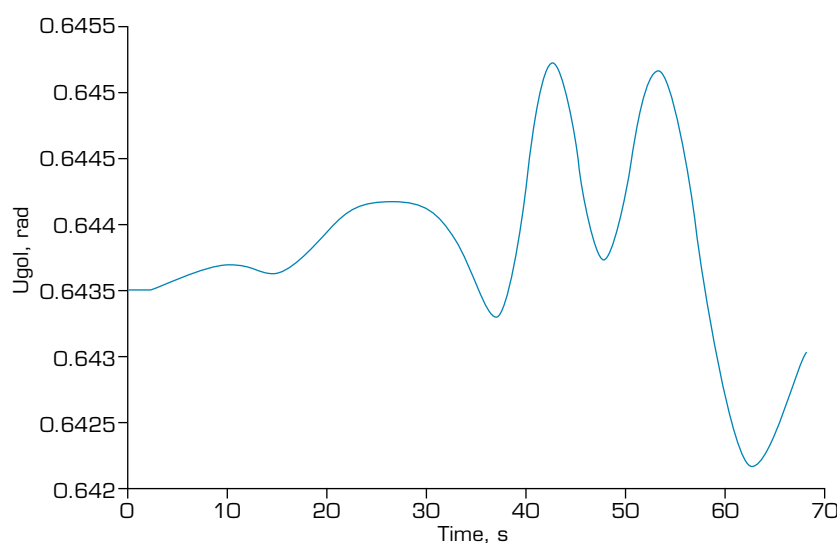
Source: Elaborated by the authors.

Figure 7. Variation of the tether's length and modification in the current distance from the UAV to the presumed landing location $L = \sqrt{x^2 + z^2}$.



Source: Elaborated by the authors.

Figure 8. UAV velocities projections.



Source: Elaborated by the authors.

Figure 9. Variation in angle α ($\pm 0,015$ rad).

DISCUSSION

Under conditions of increasing wind force with changes in the UAV's height, an algorithm for its landing has been proposed, including: attraction of UAV along a straight line connecting the points of attachment of the tether to the UAV and the wheeled UGV, achieved through the formation of a control voltage in the form of the sum of the main voltage, countering the wind force at each height and the voltage controlling the winding of the tether, which is proportional to the main voltage with a predetermined proportionality coefficient; and the formation of the lift in the UAV engines from the main constant force, compensating for its weight and the vertical component of the tether tension force, along with damping forces that allow synchronization of the current tether length with the distance from the UAV to the tether attachment point on the landing site of the wheeled UGV.

Future research is planned to explore the effects of wind gusts, characterized by their known probabilistic properties, on the dynamics of UAV flight during takeoff and landing processes, following the methodology outlined in this paper.

The modeling results have confirmed the functionality of the proposed UAV landing algorithm on a moving platform under quasi-constant extreme wind conditions.

CONCLUSIONS

The analysis of the obtained results allows for the following conclusions:

- The UAV's position on the straight line connecting the tether attachment points on the UAV and the wheeled UGV, under a constant wind effects, is stable according to the Lyapunov stability criterion. Thus, with an initial deviation of UAV of 1 m horizontally and 0.5 m vertically, after several oscillations, it returns to the equilibrium position at the coordinates related by the equation of the indicated line (Fig. 3);
- Based on preliminary numerical estimates, it has been possible to divide the initial general system of equations of motion of the UAV and TM into two independent systems. For each of these, an analytical solution has been obtained and, based on the desired landing time, preliminary control coefficients in the TM engine and damping forces in the UAV engines have been selected;
- For the simulation, the initial values of UAV and TM parameters were taken to be the same as in (Aleshin *et al.* 2020): $\cos\alpha_0 = 0.8$; $J = 0.7 \text{ kgm}^2$; $m = 6 \text{ kg}$; $c_{dz} = 0.15$; $c_{dx} = 0.12$; $c_{cef} = 0.016 \text{ Vs/rad}$; $F_w = 30 \text{ N}$; $\varepsilon = 3 \cdot 10^{-3} \text{ Nm/rad}$; $n = 0.5 \text{ Nm/A}$; $I_0 = 25 \text{ m}$.
- The landing time has been selected considering: ensuring the UAV's quasi-stationary motion during landing; acceptability for practical implementation; energy costs during the formation of voltage on the TM engine and in engines that create thrust;
- A simulation of the solution of the complete equations of UAV motion during landing has been carried out, and numerical synthesis of piecewise linear damping coefficients has been conducted by selecting the moments in time of change of their slope from the condition of synchronization of the current values of the cable length and the distance from the UAV's location during the movement to the point of the expected landing.

In this case, from the initial height $z_1 = 15 \text{ m}$ to the height $z_3 = 5 \text{ m}$ landing occurs due to the operation of TM by attracting UAV along a line close to $\alpha = \alpha_0$, while forming the value of the control voltage $U = k_u U_0(z)$ is carried out in accordance with the change in wind strength with height, and the coefficient k_u is constant throughout the entire movement up to the height $z_2 = 3 \text{ m}$ at which the wind force is practically zero (Fig. 5). In this case, the damping forces $f_{zd}z$ and $f_{xd}x$, continue to form in the UAV engines to ensure synchronization of the current cable length and the UAV position. The speed of UAV gradually decreases and its position stabilizes due to the stability of UAV position relative to the straight line $\alpha = \alpha_0$. The UAV hovers, after which further landing is carried out with the TM engine turned off, only due to the operation of the standard UAV engine control system. The corresponding Figs. of the change in UAV coordinates are presented in the Figs. 6–9.

CONFLICT OF INTEREST

Nothing to declare.

AUTHOR CONTRIBUTIONS


Conceptualization: Kuris E, Lelkov K, and Khorev T; **Data curation:** Kuris E, Lelkov K, and Khorev T; **Formal analysis:** Kuris E, Lelkov K, and Khorev T; **Acquisition of funding:** Kuris E, Lelkov K, and Khorev T; **Research:** Kuris E, Lelkov K, and Khorev T; **Methodology:** Kuris E, Lelkov K, and Khorev T; **Project administration:** Kuris E, Lelkov K, and Khorev T; **Supervision:** Kuris E, Lelkov K, and Khorev T; **Validation:** Kuris E, Lelkov K, and Khorev T; **Writing - Preparation of original draft:** Kuris E, Lelkov K, and Khorev T; **Writing - Proofreading and editing:** Kuris E, Lelkov K, and Khorev T; **Final approval:** Kuris E, Lelkov K, and Khorev T.



DATA AVAILABILITY STATEMENT

All data sets were generated or analyzed in the current study.

FUNDING

Russian Science Foundation 
Grant No. 23-29-00958

ACKNOWLEDGEMENTS

Not applicable.

REFERENCES

- Aleshin BS, Chernomorsky AI, Kuris ED, Lelkov KS, Ivakin MV (2020) Robotic complex for inspection of the outer surface of the aircraft in its parking lot. *Incas Bull* 12:21-31. <https://doi.org/10.13111/2066-8201.2020.12.S.2>
- Alonso Tabares D, Mora-Camino F (2017) Aircraft ground handling: analysis for automation. Paper presented 2020 17th AIAA Aviation Technology, Integration, and Operations Conference. AIAA; Denver, USA. <https://doi.org/10.2514/6.2017-3425>
- Antonov DA, Veremeenko KK, Zharkov MVE, Kuznetsov IM, Pron'kin AN (2017) Fault-tolerant airport vehicle integrated navigation system. Paper presented 2017 24th Saint Petersburg International Conference on Integrated Navigation Systems. State Research Center of the Russian Federation. Concern Central Scientific and Research Institute Elektropribor; St. Petersburg, Russia. <https://doi.org/10.23919/ICINS.2017.7995620>
- Arellano-Muro CA, Luque-Vega LE, Castillo-Toledo B, Loukianov AG (2013) Backstepping control with sliding mode estimation for a hexacopter. Paper presented 2013 10th International Conference on Electrical Engineering, Computing Science and Automatic Control. Instituto Politécnico Nacional and the Departments of Automatic Control; Mexico City, Mexico. <https://doi.org/10.1109/ICEEE.2013.6676026>
- Cantelli L, Presti ML, Mangiameli M, Melita CD, Muscato G (2013) Autonomous cooperation between UAV and UGV to improve navigation and environmental monitoring in rough environments. Paper presented 10th International Symposium on Humanitarian Demining coupled with the 11th IARP WS HUDEM. IARP; Sibenik, Croatia. https://www.researchgate.net/publication/303245963_Autonomous_Cooperation_between_UAV_and_UGV_to_improve_navigation_and_environmental_monitoring_in_rough_environments
- Chodnicki M, Siemiatkowska B, Stecz W, Stępień S (2022) Energy efficient UAV flight control method in an environment with obstacles and gusts of wind. *Energ* 15(10):3730. <https://doi.org/10.3390/en15103730>
- Kim P, Price LC, Park J, Cho YK (2019) UAV-UGV cooperative 3D environmental mapping. Paper presented ASCE International Conference on Computing in Civil Engineering 2019. American Society of Civil Engineers, Reston, VA.
- Krishnakumar R, Rasheed AM, Kumar KS (2015) Enhanced hover control of quad tilt frame UAV under windy conditions. *Int J Adv Robot Syst* 12(10):146. <https://doi.org/10.5772/61231>

- Liu Z, Wen S, Huang G, Li S, Deng Z (2024) Agricultural UAV obstacle avoidance system based on a depth image inverse projection algorithm and b-spline curve trajectory optimization algorithm. *Inf Techn and Contr* 53(3):736-757. <https://itc.ktu.lt/index.php/ITC/article/view/36021>
- Massera JL, Schäffer JJ (1958) Linear differential equations and functional analysis, I. *Annals of Math* 67(3):517-573. <https://doi.org/10.2307/1969871>
- Pukdeboon C (2011) A review of fundamentals of Lyapunov theory. *J Appl Sci* 10(2):55-61. https://www.researchgate.net/publication/267976343_A_Review_of_Fundamentals_of_Lyapunov_Theory
- Tikhonov AN, Goncharsky AV, Stepanov VV, Yagola AG (1995) Numerical methods for the approximate solution of ill-posed problems on compact sets. Amsterdam: Springer.
- Turgut ET, Usanmaz Ö (2016) An analysis of vertical profiles of wind and humidity based on long-term radiosonde data in Turkey. *Anadolu Univ J Sci and Techn A-Appl Sci and Eng* 17(5):830-844. <https://doi.org/10.18038/aubtda.279852>
- Uzun M, Oktay T (2023) Simultaneous UAV having actively sweep angle morphing wing and flight control system design. *Aircr Eng and Aerosp Techn* 95(3):1062-1068. <https://doi.org/10.1108/AEAT-09-2022-0259>
- Veremeenko KK, Zharkov MV, Kuznetsov IM, Pron'kin AN (2020) Strapdown inertial navigation system transfer alignment: algorithmic features and simulation performance analysis. *Russ Aeronaut* 63:618-626. <https://doi.org/10.3103/S106879982004008X>
- Veremeenko KK, Zharkov MV, Kuznetsov IM, Pron'kin AN (2021) Investigation of parametric uncertainty influence on accuracy of strapdown inertial navigation system transfer alignment. *Russ Aeronaut* 64:518-525. <https://doi.org/10.3103/S106879982103020X>
- Wang B, Ali ZA, Wang D (2020) Controller for UAV to oppose different kinds of wind in the environment. *J Contr Sci and Eng* 2020(1):5708970. <https://doi.org/10.1155/2020/5708970>
- Wang L, Cheng D, Gao F, Cai F, Guo J, Lin M, Shen S (2020) A collaborative aerial-ground robotic system for fast exploration. Paper presented 2018 International Symposium on Experimental Robotics. International Foundation of Robotics Research; Buenos Aires, Argentina. https://doi.org/10.1007/978-3-030-33950-0_6
- Xie J, Huang J, Song L, Fu J, Lu X (2022) An effort saving method to establish global aerodynamic model using CFD. *Aircr Eng and Aerosp Techn* 94(11):1-19. <https://doi.org/10.1108/AEAT-10-2021-0299>
- Zharkov MV, Veremeenko KK, Kuznetsov IM, Pronkin AN (2022) Experimental results of attitude determination functional algorithms implementation in strapdown inertial navigation system. *Sensors* 22(5):1849. <https://doi.org/10.3390/s22051849>